Nanoparticle Surface Chemistry

DOI: 10.1002/anie.201208331

Spatial Charge Configuration Regulates Nanoparticle Transport and Binding Behavior In Vivo**

*Hee-Sun Han, John D. Martin, Jungmin Lee, Daniel K. Harris, Dai Fukumura, Rakesh K. Jain, and Moungi Bawendi**

Nanoparticles are widely used as imaging probes[1] or as drug carriers,[2] however, the design rules to guide their properties for in vivo application remain incomplete. Until recently, the physical characteristics of nanoparticles such as size, shape, hydrophobicity, and net charge have been mostly considered as primary handles to achieve nanoparticles with desired in vivo characteristics. However, we hypothesized that the detailed arrangement of ligands also has a strong influence on the in vivo behavior of nanoparticles, because the interactions of nanoparticles with the surrounding biomolecules or cellular structures are mediated by surface-to-surface contacts. In support of this hypothesis, previous work has shown that specific arrangements of hydrophobic ligands on the nanoparticle surface can affect the cellular uptake pathway of the particles.[3] Here, we demonstrate the influence of spatial distribution of surface charge on the binding and transport behavior of nanoparticles in vivo. An understanding of the influence of charge distribution on nanoparticle behavior is essential, as most nanoparticle coatings employ charged functional groups for further conjugation with biomolecules or drugs. Even though there have been reports on nanoparticles employing uncharged functional groups for conjugations,[4] most widely used conjugation methods still rely on ester bond formation, amide coupling, or maleimide–thiol coupling and utilize carboxylic acid or amine groups. Furthermore, studying the influence of surface charge arrangement on nanoparticle behavior inspires the design of zwitterionic surface coatings, which were recently introduced as possible alternative for bulky nonionic polymeric surface coatings such as poly(ethylene glycol) (PEG).[5]

For this study, quantum dots (QDs) coated with newly designed betaine-functionalized poly(imidazole) ligands (BPILs) were utilized. The unique optical properties of QDs[6] allow facile analysis of QD behavior by using optical microscopes, rather than elemental analysis,[7] magnetic resonance imaging,[8] or electron microscopy,[9] and simultaneous analysis of multiple targets. Recent advances in the development of nonionic or charged surface coatings enabled preparation of high-quality QDs in aqueous buffers.[10] However, most zwitterionic surface coatings for QDs that are currently reported employ thiol as a binding group[5a,b,11] and thus suffer from poor stability in ambient condition owing to the oxidation of thiols and significant nonspecific binding to serum proteins.[10c,11] To prepare stable and biocompatible zwitterionic QDs, we designed new zwitterionic coatings containing multiple imidazole moieties, which are chemically stable, as cooperative binding groups to the QD surface. In addition to an enhanced solution stability, the new zwitterionic QDs have other potential advantages such as a compact size, a narrow polydispersity index of the polymer, straightforward modulation of charge density and charge distribution, and minimal nonspecific binding towards cells and proteins.

BPILs, random copolymers employing imidazole groups for QD binding and sulfobetaine or carboxybetaine groups for water solubilization, are synthesized in three steps (Scheme 1): 1) RAFT-mediated polymerization of the backbone (**3**), 2) betainization of the polymers (**4**, **6**), and 3) cleavage of *tert*-butyloxycarbonyl (Boc) protecting groups (**5**, **7**). RAFT-mediated polymerization allows tight control over the mean and standard deviation of the resulting polymer weights (Figure S5 in the Supporting Information). Postmodification of a polymerized backbone by using highly strained 1,3-propane sultone and β-propiolactone enables one-step conversion of tertiary amines to sulfobetaine or carboxybetaine by releasing the ring strain. The net charge and degree of freely exposed amines of BPILs were controlled by tuning the conversion efficiencies of tertiary amines to betaine moieties.

[*] Dr. H.-S. Han, J. Lee, Prof. Dr. M. Bawendi
Department of Chemistry, Massachusetts Institute of Technology
Cambridge, MA 02139 (USA)
E-mail: mgb@mit.edu
J. D. Martin, Prof. Dr. D. Fukumura, Prof. Dr. R. K. Jain
Edwin L. Steele Laboratory, Department of Radiation Oncology
Massachusetts General Hospital and Harvard Medical School
Boston, MA 02114 (USA)
J. D. Martin
Department of Chemical Engineering
Massachusetts Institute of Technology
Cambridge, MA 02139 (USA)
D. K. Harris
Department of Materials Science and Engineering
Massachusetts Institute of Technology
Cambridge, MA 02139 (USA)

[**] The research work is supported by the U.S. National Institute of Health grants, P01-CA080124 (R.K.J and D.F.), R01-CA085140 (R.K.J.), R01-CA096915 (D.F.), R01-CA115767 (R.K.J.), R01-CA126642 (R.K.J.), U54-CA151884 (M.G.B.), R01-CA126642 (M.G.B.), Federal Share Proton Beam Program Income (R.K.J.), and T32-CA073479 (R.K.J.); by the MIT DCIF CHE-9808061, DBI-9729592; by the ISN W911NF-07-D-0004 (M.G.B); by the NSF-MRSEC program DMR-0117795 through the use of its shared user facilities; and by DoD Breast Cancer Research Innovator award (W81XWH-10-1-0016 (R.K.J.). H.-S.H. was supported by the Samsung Scholarship. We would like to thank Julia Kahn for technical assistance.

Supporting information for this article is available on the WWW under http://dx.doi.org/10.1002/anie.201208331.

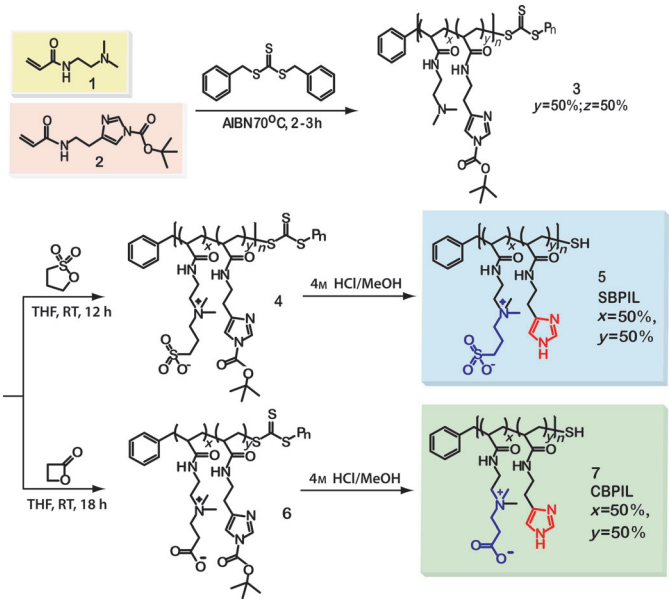

Scheme 1. Scheme for synthesis of sulfobetaine- and carboxybetaine-functionalized poly(imidazole) ligands (SBPILs and CBPILs). Random copolymer backbones (**3**) are synthesized through radical addition fragmentation chain transfer (RAFT)-mediated polymerization and betainized using 1,3-propanesultone and β-propiolactone to yield SBPILs (**5**) and CBPILs (**7**), respectively. AIBN = azobisisobutyronitrile.

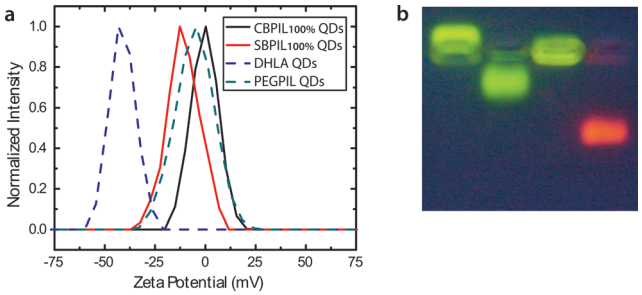

Figure 1. Surface net charge measurements. a) Zeta potential measurements illustrate that SBPIL QDs are slightly negative and CBPIL QDs are neutral. Zeta potential measurements for DHLA QDs (QDs coated with dihydrolipoic acid, highly negative) and PEGPIL QDs (QDs coated with poly(ethylene glycol)-functionalized PILs, nonionic) are shown as a reference. b) Gel electrophoresis of the PEGPIL QDs (first lane), SBPIL QDs (second lane), CBPIL QDs (third lane), and DHLA QDs (fourth lane) confirm the zeta potential measurement.

Water-soluble QDs coated with the BPILs (BPIL QDs) were prepared by exchanging the native hydrophobic ligands with BPILs. Various types of QDs emitting from the near infrared to the visible were successfully brought into water with both sulfobetaine-functionalized poly(imidazole) ligands (SBPILs) and carboxybetaine-functionalized poly(imidazole) ligands (CBPILs): InAs/CdZnS emitting at 750 nm (QD_{750}), CdSe/CdS emitting at 570 nm (QD_{570}), and CdSe/CdZnS emitting at 612 nm (QD_{612}). Owing to multidentate imidazole binding units, BPIL QDs exhibit greatly enhanced stability across a wide pH range (Figure S10 in the Supporting Information). In addition, both CBPIL and SBPIL QD solutions were stable under ambient conditions for over a month, which is a significant enhancement over the hours to days shelf lives of reported zwitterionic QDs.[5a,b] Greatly enhanced stability of BPIL QDs allowed in-depth analysis of the in vivo behavior of zwitterionic QDs.

The net charge of SBPIL QDs and CBPIL QDs was characterized by measuring the zeta potential and by performing gel electrophoresis. The zeta potential of QDs coated with CBPIL with 100% conversion of tertiary amines to carboxybetaine moieties ($CBPIL_{100\%}$ QDs) was approximately 0.3 mV (close to neutral), and that of $SBPIL_{100\%}$ QDs was approximately −13.1 mV (mildly negatively charged; Figure 1). The measured negative charge of SBPIL QDs, despite the zwitterionic nature of the SBPILs, can be explained by association of negative ions present in buffers with the quaternary amines in SBPILs (see results in the Supporting Information).[5e] The net charge of SBPIL QDs was tuned by adjusting betainization efficiencies. Neutral QDs were prepared by using $SBPIL_{80\%}$ (80% conversion efficiency; see Table S1 in the Supporting Information).

To verify the influence of spatial charge configuration on QD–cell interactions in vitro, nonspecific binding of zwitterionic QDs (SBPIL QDs and CBPIL QDs) with cultured HeLa cells was evaluated. Previous reports[12] predict neutral and hydrophilic QDs ($SBPIL_{80\%}$ QDs and $CBPIL_{100\%}$ QDs) to exhibit minimal cell binding. Instead, cells incubated with $SBPIL_{80\%}$ QDs and $CBPIL_{100\%}$ QDs displayed a significant increase of fluorescence signal, thus suggesting nonspecific binding of the QDs to cells (Figure 2a, b and Figure S13 in the Supporting Information). In addition, dramatic differences in nonspecific cell binding were observed depending on the betainization efficiencies of the SBPILs (Figure 2a).

The results with SBPIL QDs illustrate that, even for QDs that are neutral or slightly charged, the number of spatially exposed amines, which are positively charged groups, is an important factor that determines the level of nonspecific binding to cells. $SBPIL_{80\%}$ QDs possessing nonconverted tertiary amines exhibited significant nonspecific binding to cells despite the zero net charge of the particle, while $SBPIL_{100\%}$ QDs with no exposed amines showed virtually no binding to cells despite their small negative charge.

In vitro nonspecific binding results with CBPIL QDs reinforce the importance of the absence of positively charged groups on the outermost layer to achieve minimal nonspecific cell adsorption. Even though the chemical structure of $CBPIL_{100\%}$ indicates that the tertiary amine groups are fully converted to carboxybetaine moieties and thereby well-screened by negative carboxylate groups, quaternary amines are more likely to be in the outermost layer (exposed) than carboxylate groups owing to the affinity of carboxylate to the QD surface. The binding affinity of carboxylic acids to the QD surface is similar to that of imidazole groups, which are anchoring groups in BPILs.[13] Therefore, both carboxylic acids and imidazole moieties are expected to bind to the QD surface. Attraction of carboxylate groups towards the QD surface has been previously confirmed.[14] The high level of exposed amines resulted in significant nonspecific binding for $CBPIL_{100\%}$ QDs despite their nearly neutral charge (zeta

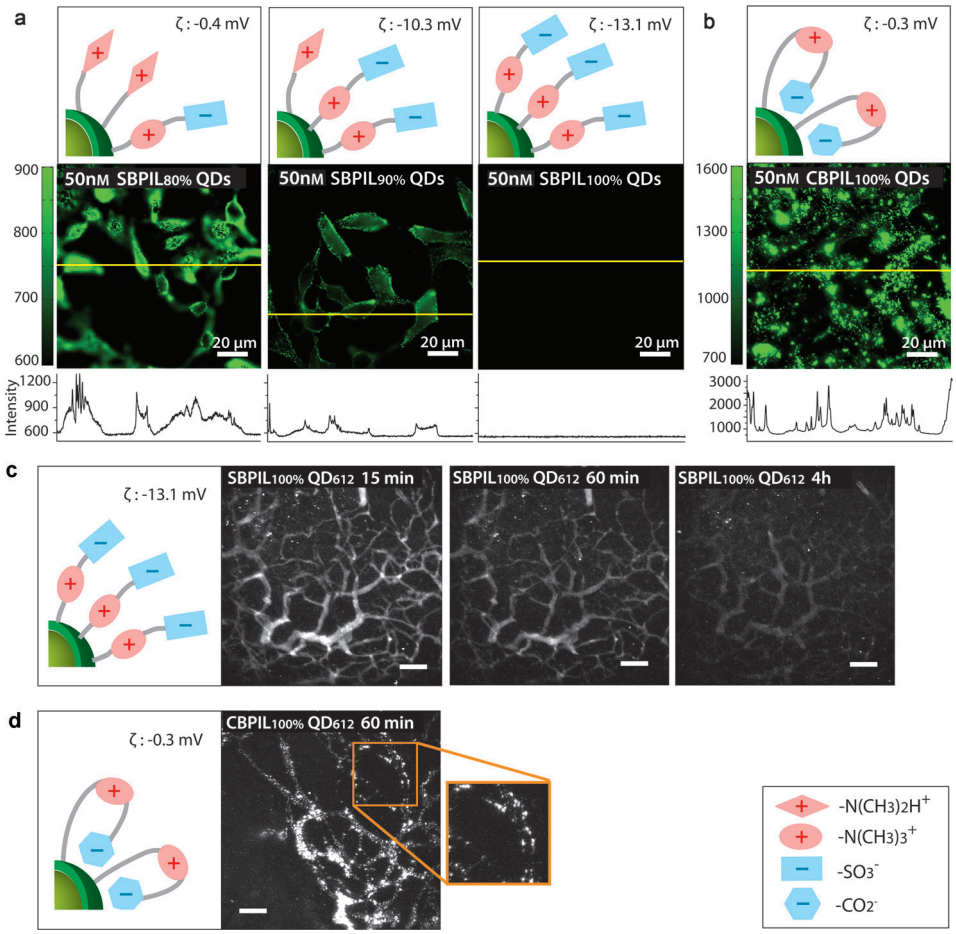

Figure 2. Influence of charge distribution on nonspecific binding of QDs in vitro and in vivo. Cartoons of the QD surface are included to illustrate expected charge distribution on QDs for each sample. Charge distributions in the surface coatings were inferred from the different affinities of carboxylate groups and sulfonate groups towards QD surfaces. a, b) Influence of surface charge distribution on nonspecific binding to HeLa cells. Exposure time = 100 ms. Yellow lines indicate where the intensity profile was measured. Refer to Figure S12 in the Supporting Information for the images replotted by using a heatmap for better visualization of the QD signal. a) Significant decrease of the nonspecific binding is observed when the betainization efficiencies increases from 80% to 100% for SBPIL QDs. The data show that exposed free amines (positively charged groups) trigger nonspecific binding to cells. b) $CBPIL_{100\%}$ QDs exhibit a high level of nonspecific binding owing to exposed amine groups. $CBPIL_{100\%}$ QDs display significantly higher nonspecific binding to cells than SBPIL QDs. Note the change in the intensity scale of the plot below the picture. c, d) Influence of charge distribution on in vivo clearance. c) Clearance of SBPIL QD_{612} from the vessels. The vessels of E0771 murine mammary adenocarcinoma grown in SCID mice (SCID = severe combined immunodeficiency) were imaged by multiphoton microscopy through a mammary fat pad window at 15 min, 60 min, and 4 h after intravenous injection. Note that SBPIL QD_{612} clears from the vessels without leaving any evidence of nonspecific accumulation. Scale bar = 100 μm. d) Clearance of $CBPIL_{100\%}$ QDs from the vessels. An image taken at 60 min after the injection of $CBPIL_{100\%}$ QDs illustrates that $CBPIL_{100\%}$ QDs accumulate on the vessel walls nonspecifically.

potential of −0.3 mV; Figure 2b). $CBPIL_{100\%}$ QDs also exhibited strong interaction with diverse polymeric beads such as sephadex, superpose, sephacryl, and superdex. In contrast, the quaternary amines on $SBPIL_{100\%}$ QDs are well-screened from the environment by the sulfonates, as sulfonate groups do not interact with the QD surface. Minimal nonspecific binding was observed for $SBPIL_{100\%}$ QDs.

Previous studies on gold surfaces (both nanoparticles and flat substrates) coated with carboxybetaine ligands[15] also confirm our observation that spatially exposed positive charges trigger the high level of nonspecific binding. Unlike for $CBPIL_{100\%}$ QDs, carboxybetaine ligands are anchored to the gold substrates through thiols. Since the binding affinity of thiols to gold is far greater than that of carboxylate groups,[16] the entire carboxybetaine moieties are exposed to the environment, that is, positive amine groups are well-screened by negative carboxylate groups. Therefore, gold substrates coated with carboxybetaine ligands are reported to exhibit extremely low nonspecific binding properties to cells and proteins.[5e,15b,17]

The influence of the relative distribution of charges on nonspecific binding of nanoparticles in vivo was evaluated by injecting $SBPIL_{100\%}$ QDs and $CBPIL_{100\%}$ QDs intravenously into mice and monitoring the vessels over time. Upon systemic administration, $SBPIL_{100\%}$ QDs, which are likely to display negative charges on their outermost layer, cleared from vessels without leaving any evidence of nonspecific accumulation. In contrast, $CBPIL_{100\%}$ QDs, which are likely to display positive charge in their outermost layer, -accumulated on vessels nonspecifically (Figure 2c, d). Electrostatic interactions between the exposed positive charges on CBPIL QDs and negatively charged groups presented on the surface of endothelial cells may trigger nonspecific accumulation of $CBPIL_{100\%}$ QDs.

Furthermore, we compared the in vivo binding and transport behavior of zwitterionic QDs versus nonionic QDs to study the influence of the existence of charge in neutral nanoparticles. $SBPIL_{100\%}$ QDs were chosen to represent zwitterionic QDs owing to their low nonspecific binding properties, and PEGPIL QDs (QDs coated with poly(ethylene glycol)-functionalized PILs) were selected as an example of nonionic QDs. Previously reported PEGPILs[10c] have the same polymer structure as BPILs except the water-solubilizing groups and therefore serve as an ideal control pair for BPIL QDs.

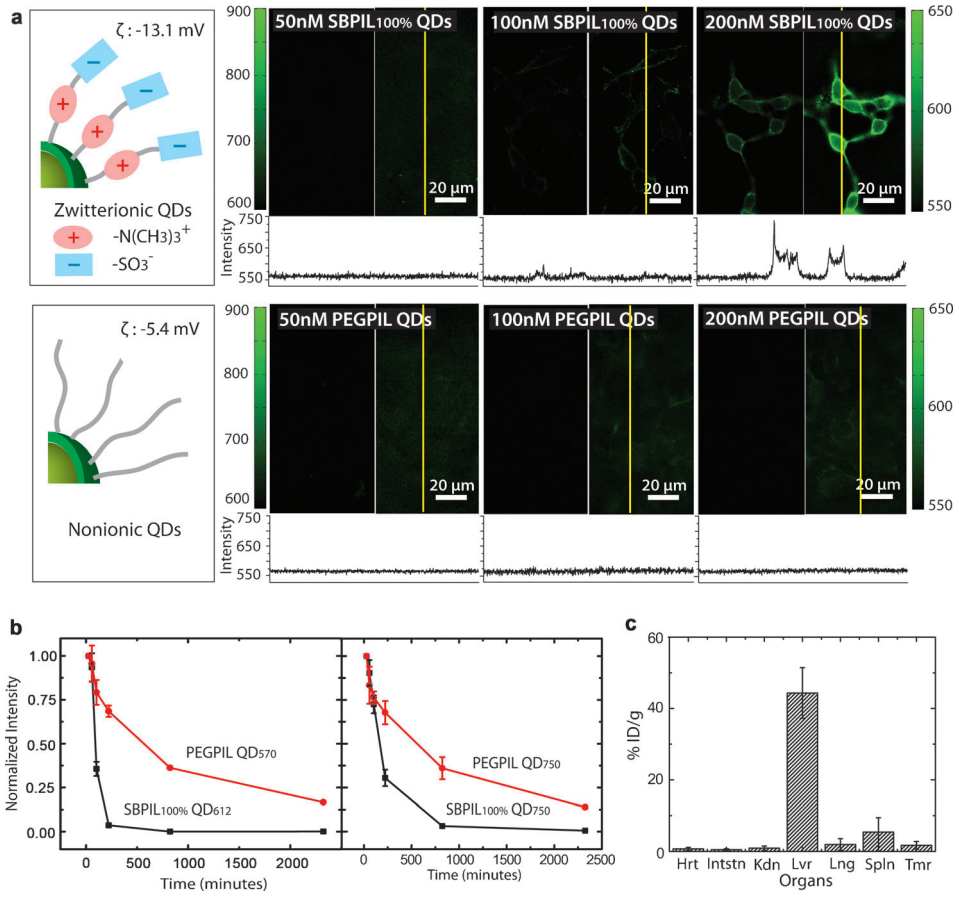

Figure 3. Comparison of in vitro and in vivo behavior of zwitterionic QDs versus nonionic QDs. a) Comparison of in vitro nonspecific binding to HeLa cells. Zwitterionic QDs exhibited slightly higher nonspecific cell binding than nonionic QDs. Even though virtually no binding is observed for $SBPIL_{100\%}$ QDs at 50 nM or lower, the level of nonspecific binding increases with higher concentrations of QDs (top). In contrast, the level of nonspecific binding for PEGPIL QDs remains minimal up to 200 nM (bottom). The intensity scale bars shown on the left and right correspond to the left and right parts of the images, respectively. The vertical lines in the right parts of the images indicate where the intensity profile shown below was measured. Refer to Figure S12 in the Supporting Information for the images replotted by using a heatmap for better visualization of the QD signal. b) Comparison of clearance kinetics. Clearance kinetics of SBPIL QD_{612} and PEGPIL QD_{570} (left panel), which have very similar hydrodynamic diameters, and SBPIL QD_{750} and PEGPIL QD_{750} (right panel), that were synthesized with the same QD cores. Both results illustrate that SBPIL QDs clear from the vessels much faster than PEGPIL QDs. c) Biodistribution (%ID/g tissue; ID = injected dose) of zwitterionic QDs 24 h after QD injection shown for different organs and the tumor. SBPIL QDs are cleared through liver and spleen, which may indicate RES clearance (RES = reticuloendothelial system). Abbreviations used are: Hrt, heart; Intstn, intestine; Kdn, kidney; Lvr, liver; Lng, lung; Spln, spleen; and Tmr, tumor. Error bars represent 95% confidence interval.

In vitro nonspecific binding tests show that zwitterionic QDs exhibit slightly higher nonspecific binding to cells and serum proteins. $SBPIL_{100\%}$ QDs exhibited slightly higher nonspecific cell adsorption than PEGPIL QDs at concentrations above 100 nM (Figure 3a), even though virtually no binding was observed for both $SBPIL_{100\%}$ QDs and PEGPIL QDs at concentrations of 50 nM or lower. Also, when incubating with varying concentrations of fetal bovine serum (FBS), $SBPIL_{100\%}$ QDs exhibit weak nonspecific binding to serum proteins at high concentrations of FBS (Figure S14 in the Supporting Information), while a previous report on PEGPIL QDs show virtually no binding up to 0.90 × serum.[10c] These results suggest that long, flexible, and nonionic PEG chains are more effective than compact and ionic betaine groups at preventing biomolecules from being adsorbed nonspecifically—they physically protect the surface better.

Analysis of the clearance kinetics of zwitterionic QDs and nonionic QDs shows that zwitterionic QDs clear from blood significantly faster than nonionic QDs. When zwitterionic QDs ($SBPIL_{100\%}$ QD_{612}) and nonionic QDs (PEGPIL QD_{570}) with similar net charge (−5.4 mV for PEGPIL QDs, −13.1 mV for $SBPIL_{100\%}$ QDs) and hydrodynamic sizes (ca. 10 nm, Figure S16 in the Supporting Information) were co-injected into mice, zwitterionic QDs cleared an order of magnitude faster than nonionic QDs (Figure 3b, left panel). We confirmed that this result is solely due to the difference in the coatings and not due to the variability of the QD cores by measuring clearance kinetics of $SBPIL_{100\%}$ QD_{750} and PEGPIL QD_{750} (Figure 3b, right panel). The fast clearance of zwitterionic QDs might be due to an immune response triggered by weak nonspecific binding to serum proteins. Biodistribution analysis using inductively coupled plasma mass spectroscopy (ICP-MS) confirms the reticuloendothelial system (RES) clearance of the particles; most of $SBPIL_{100\%}$ QDs are cleared through liver and spleen (Figure 3c and Figure S17 in the Supporting Information).

Lastly, tumor transport measurements showed that nonionic QDs extravasate from vessels and diffuse into tumor an order of magnitude faster than zwitterionic QDs displaying negatively charged groups in their outermost layer. Transvascular transport of QDs in tumors was assessed by measuring effective permeability[18] of the particles in two different types of breast tumors: E0771 and MCaIV. The effective permeability measures the ability of QDs to extravasate from vessels and diffuse into the extravascular space, and is independent of clearance rate. Of the two breast tumor types, MCaIV has exceptionally large pores. The average pore cutoff size of MCaIV is 1.2 to 2 μm, while most tumors show a pore cutoff size of 380 to 780 nm.[19] In both

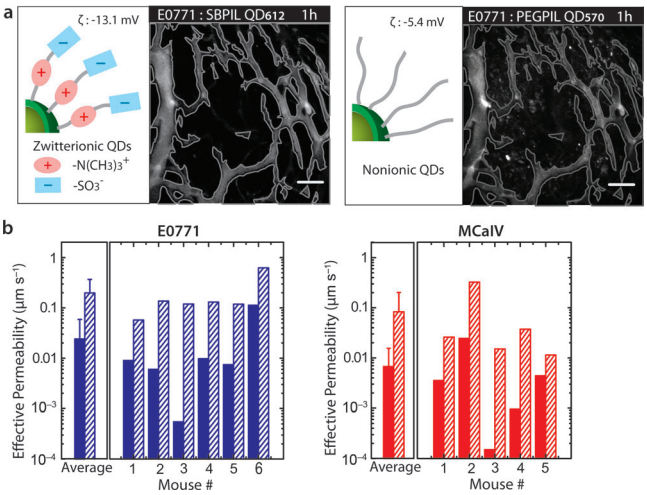

Figure 4. Comparison of transvascular transport of zwitterionic QDs versus nonionic QDs in breast cancers. a) Real-time intravital microscopy of ligand-dependent nanoparticle distribution in a murine breast tumor. A mixture of SBPIL QD_{612} (left panel) and PEGPIL QD_{570} (right panel), which has the same hydrodynamic diameter, was injected intravenously into an SCID mouse bearing an E0771 murine mammary adenocarcinoma in a mammary fat pad chamber. Angiographic images demonstrate distribution of the nanoparticles one hour after injection. The initial fluorescence was recorded shortly after injection, and is depicted as the gray line. The images show that $SBPIL_{100\%}$ QD_{612} extravasate from vessels significantly less than PEGPIL QD_{570}. Images are maximum intensity projections of 3D volumes. Scale bar = 100 μm. b) Effective permeability of SBPIL QD_{570} and PEGPIL QD_{612} in mice bearing an E0771 murine mammary adenocarcinoma (left) and a MCaIV murine mammary adenocarcinoma (right). Solid bars represent the values obtained with SBPIL QD_{612}. Lined bars represent the values obtained with PEGPIL QD_{570}. Error bars represent 95% confidence interval. In both tumor models, SBPIL QD_{612} always showed significantly smaller effective permeability than PEGPIL QD_{570}.

tumor models, the zwitterionic QDs exhibited an effective permeability that was one to two orders of magnitude lower than nonionic QDs (Figure 4). The unexpectedly low effective permeability of $SBPIL_{100\%}$ QDs is likely due to the combination of the exposed negative charge (the molecular arrangement of charges) and the weak negative net charge (net physical property) of $SBPIL_{100\%}$ QDs. Both the net negative charge and the exposed negative surface charge of SBPIL QDs may cause the QDs to be repelled from endothelial cells, which are known to display negatively charged groups on their surface.[20] It is striking that the combination of different charge configurations and a small difference in the net charge (−5.4 mV versus −13.1 mV) yield significantly different tumor transport behavior.

In this study, we designed and synthesized a new class of zwitterionic QD ligands to prepare neutral QDs with modulated spatial charge arrangements. Greatly enhanced stability and the low biofouling of BPIL QDs allowed an in-depth analysis of in vivo behavior. Our study demonstrates the critical importance of spatial charge arrangements in determining in vivo characteristics of nanoparticles. Zwitterionic QDs displaying positive charges in their outermost layer exhibit significant nonspecific accumulation to cultured cells and vessels in live mice, whereas zwitterionic QDs displaying negative charges in their outermost layer show minimal nonspecific adsorption. In addition, comparison of in vivo behavior between zwitterionic QDs and nonionic QDs illustrate that exposed charged groups cause an enhanced interaction of zwitterionic QDs with their environment and result in significantly different binding and transport behavior in vivo. Therefore, when designing nanoparticles for in vivo applications, the three-dimensional configuration of charges needs to be closely considered with specific applications in mind. For instance, to minimize nonspecific interaction of nanoparticles with their environment, positively charged groups need to be spatially screened. In addition, the development of new conjugation methods employing neutral functional groups is highly recommended for achieving nanoparticles with long blood circulation and rapid transvascular delivery. These findings can be extended to other substrates, inorganic particles, and polymeric nanoparticles that can be used as imaging agents or drug carriers.

Received: October 17, 2012
Revised: November 16, 2012
Published online: December 17, 2012

Keywords: cancer · ligand design · nanoparticles · quantum dots · zwitterions

[1] a) M. Bruchez, Jr., M. Moronne, P. Gin, S. Weiss, A. P. Alivisatos, *Science* **1998**, *281*, 2013–2016; b) W. C. W. Chan, S. Nie, *Science* **1998**, *281*, 2016–2018; c) J. B. Delehanty, C. E. Bradburne, K. Susumu, K. Boeneman, B. C. Mei, D. Farrell, J. B. Blanco-Canosa, P. E. Dawson, H. Mattoussi, I. L. Medintz, *J. Am. Chem. Soc.* **2011**, *133*, 10482–10489; d) F. Pinaud, S. Clarke, A. Sittner, M. Dahan, *Nat. Methods* **2010**, *7*, 275–285.

[2] a) D. A. LaVan, T. McGuire, R. Langer, *Nat. Biotechnol.* **2003**, *21*, 1184–1191; b) I. Brigger, C. Dubernet, P. Couvreur, *Adv. Drug Delivery Rev.* **2002**, *54*, 631–651.

[3] A. Verma, O. Uzun, Y. H. Hu, Y. Hu, H. S. Han, N. Watson, S. L. Chen, D. J. Irvine, F. Stellacci, *Nat. Mater.* **2008**, *7*, 588–595.

[4] a) H.-S. Han, N. K. Devaraj, J. Lee, S. A. Hilderbrand, R. Weissleder, M. G. Bawendi, *J. Am. Chem. Soc.* **2010**, *132*, 7838–7839; b) N. K. Devaraj, R. Upadhyay, J. B. Haun, S. A. Hilderbrand, R. Weissleder, *Angew. Chem.* **2009**, *121*, 7147–7150; *Angew. Chem. Int. Ed.* **2009**, *48*, 7013–7016; c) C. Hein, X.-M. Liu, D. Wang, *Pharm. Res.* **2008**, *25*, 2216–2230.

[5] a) W. Liu, H. S. Choi, J. P. Zimmer, E. Tanaka, J. V. Frangioni, M. Bawendi, *J. Am. Chem. Soc.* **2007**, *129*, 14530–14531; b) E. Muro, T. Pons, N. Lequeux, A. Fragola, N. Sanson, Z. Lenkei, B. Dubertret, *J. Am. Chem. Soc.* **2010**, *132*, 4556–4557; c) R. E. Holmlin, X. Chen, R. G. Chapman, S. Takayama, G. M. Whitesides, *Langmuir* **2001**, *17*, 2841–2850; d) S. Chen, J. Zheng, L. Li, S. Jiang, *J. Am. Chem. Soc.* **2005**, *127*, 14473–14478; e) J. Ladd, Z. Zhang, S. Chen, J. C. Hower, S. Jiang, *Biomacromolecules* **2008**, *9*, 1357–1361.

[6] a) B. O. Dabbousi, J. Rodriguez-Viejo, F. V. Mikulec, J. R. Heine, H. Mattoussi, R. Ober, K. F. Jensen, M. G. Bawendi, *J. Phys. Chem. B* **1997**, *101*, 9463–9475; b) M. Bruchez, Jr., M. Moronne, P. Gin, S. Weiss, A. P. Alivisatos, *Science* **1998**, *281*, 2013–2016; c) Z. A. Peng, X. Peng, *J. Am. Chem. Soc.* **2001**, *123*, 183–184.

[7] J. Xie, C. Xu, N. Kohler, Y. Hou, S. Sun, *Adv. Mater.* **2007**, *19*, 3163–3166.

[8] A. L. Martin, L. M. Bernas, B. K. Rutt, P. J. Foster, E. R. Gillies, *Bioconjugate Chem.* **2008**, *19*, 2375–2384.

[9] B. D. Chithrani, A. A. Ghazani, W. C. W. Chan, *Nano Lett.* **2006**, *6*, 662 – 668.
[10] a) M. S. Nikolic, M. Krack, V. Aleksandrovic, A. Kornowski, S. Förster, H. Weller, *Angew. Chem.* **2006**, *118*, 6727 – 6731; *Angew. Chem. Int. Ed.* **2006**, *45*, 6577 – 6580; b) C. Geidel, S. Schmachtel, A. Riedinger, C. Pfeiffer, K. Müllen, M. Klapper, W. J. Parak, *Small* **2011**, *7*, 2929 – 2934; c) W. Liu, A. B. Greytak, J. Lee, C. R. Wong, J. Park, L. F. Marshall, W. Jiang, P. N. Curtin, A. Y. Ting, D. G. Nocera, D. Fukumura, R. K. Jain, M. G. Bawendi, *J. Am. Chem. Soc.* **2010**, *132*, 472 – 483.
[11] V. V. Breus, C. D. Heyes, K. Tron, G. U. Nienhaus, *ACS Nano* **2009**, *3*, 2573 – 2580.
[12] a) J. P. Ryman-Rasmussen, J. E. Riviere, N. A. Monteiro-Riviere, *Nano Lett.* **2007**, *7*, 1344 – 1348; b) E. C. Cho, J. Xie, P. A. Wurm, Y. Xia, *Nano Lett.* **2009**, *9*, 1080 – 1084; c) A. Verma, F. Stellacci, *Small* **2010**, *6*, 12 – 21.
[13] J. Y. Rempel, B. L. Trout, M. G. Bawendi, K. F. Jensen, *J. Phys. Chem. B* **2006**, *110*, 18007 – 18016.
[14] a) P. M. Allen, W. Liu, V. P. Chauhan, J. Lee, A. Y. Ting, D. Fukumura, R. K. Jain, M. G. Bawendi, *J. Am. Chem. Soc.* **2010**, *132*, 470 – 471; b) I. Medintz, H. Uyeda, E. Goldman, H. Mattoussi, *Nat. Mater.* **2005**, *4*, 435 – 446; c) J. Chen, J. L. Song, X. W. Sun, W. Q. Deng, C. Y. Jiang, W. Lei, J. H. Huang, R. S. Liu, *Appl. Phys. Lett.* **2009**, *94*, 153115.
[15] a) G. Mahmud, S. Huda, W. Yang, K. Kandere-Grzybowska, D. Pilans, S. Jiang, B. A. Grzybowski, *Langmuir* **2011**, *27*, 10800 – 10804; b) Z. Zhang, S. Chen, S. Jiang, *Biomacromolecules* **2006**, *7*, 3311 – 3315; c) W. Yang, L. Zhang, S. Wang, A. D. White, S. Jiang, *Biomaterials* **2009**, *30*, 5617 – 5621.
[16] a) D. B. Amabilino, S. D. Feyter, R. Lazzaroni, E. Gomar-Nadal, J. Veciana, C. Rovira, M. M. Abdel-Mottaleb, W. Mamdouh, P. Iavicoli, K. Psychogyiopoulou, M. Linares, A. Minoia, H. Xu, J. Puigmartí-Luis, *J. Phys. Condens. Matter* **2008**, *20*, 184003; b) G. M. Wang, W. C. Sandberg, S. D. Kenny, *Nanotechnology* **2006**, *17*, 4819; c) H. Kondoh, C. Kodama, H. Sumida, H. Nozoyec, *J. Chem. Phys.* **1999**, *111*, 1175 – 1184.
[17] W. Yang, H. Xue, W. Li, J. Zhang, S. Jiang, *Langmuir* **2009**, *25*, 11911 – 11916.
[18] E. B. Brown, R. B. Campbell, Y. Tsuzuki, L. Xu, P. Carmeliet, D. Fukumura, R. K. Jain, *Nat. Med.* **2001**, *7*, 864 – 868.
[19] a) S. K. Hobbs, W. L. Monsky, F. Yuan, W. G. Roberts, L. Griffith, V. P. Torchilin, R. K. Jain, *Proc. Natl. Acad. Sci. USA* **1998**, *95*, 4607 – 4612; b) V. P. Chauhan, T. Stylianopoulos, J. D. Martin, Z. Popovic, O. Chen, W. S. Kamoun, M. G. Bawendi, D. Fukumura, R. K. Jain, *Nat. Nanotechnol.* **2012**, *7*, 383 – 388.
[20] a) M. Simionescu, N. Simionescu, *Annu. Rev. Physiol.* **1986**, *48*, 279 – 293; b) T. Stylianopoulos, K. Soteriou, D. Fukumura, R. K. Jain, *Ann. Biomed. Eng.* **2012**, DOI: 10.1007/s10439-012-0630-4.

